STRUCTURAL RESPONSE OF A BASE-ISOLATED BUILDING SUBJECTED TO EXTREME ACTIONS

Patricia MURZEA
Lecturer, PhD Eng., Military Technical Academy "Ferdinand I", Department of Civil Engineering, Military Engineering and Geomatics, e-mail: patricia.murzea@mta.ro

Cătălin BACIU
Colonel, Associate Prof., PhD Eng., Military Technical Academy "Ferdinand I", Department of Civil Engineering, Military Engineering and Geomatics, e-mail: catalin.baciu@mta.ro

Abstract. This paper presents the results of a comprehensive analysis conducted on a reinforced concrete frame structure subjected sequentially to extreme actions, namely seismic events and explosions. The structure was evaluated under two different foundation configurations: a traditional fixed-base (rigidly embedded in the ground) and a modern base-isolated system using Lead Rubber Bearings (LRB). Structural analyses were carried out in the elastic domain: the response spectrum method was applied for seismic actions, while a linear dynamic analysis using time-history functions was employed for explosions. The results emphasize the significant contribution of the elastomeric bearings to the structural response under both types of extreme loading scenarios.

Key words: LRB, earthquake, blast.

1. Introduction

The general objective of the paper is to evaluate the dynamic behavior of a reinforced concrete frame structure subjected sequentially to extreme actions—earthquakes and explosions—under both fixed-base and base-isolated configurations, in order to highlight the contribution of the isolation system to the overall seismic and blast resilience of the structure.

To achieve this goal, the following specific objectives were defined:

1. To compare the structural response between two foundation configurations – a traditional fixed-base system and a base-isolated system using Lead Rubber Bearings (LRB).
2. To analyze the elastic behavior of the structure by applying the response spectrum method for seismic actions and a linear dynamic analysis using time-history functions for blast loading.
3. To determine the influence of base isolation on the fundamental vibration period, maximum displacements and base shear forces, in comparison with the conventional fixed-base solution.
4. To assess the effectiveness of the elastomeric bearings (LRB) in mitigating the combined effects of extreme dynamic

actions and enhancing the overall safety and functionality of the structure.

The novelty of this study lies in addressing two aspects that are scarcely explored in current literature. First, the seismic scenario considers Vrancea-type earthquakes, characterized by long-period ground motions without clear dominant frequencies—a form of seismicity that is atypical on a global scale and particularly relevant to the Romanian context. Second, the study introduces a blast loading scenario, a topic for which limited research exists regarding the efficiency of base-isolated systems. The investigation aims to determine whether elastomeric isolation devices (LRB) are capable of responding effectively within the very short duration of an explosion event and, if so, to what extent they can improve the structural response of the superstructure.

The theory of seismic isolation was first documented over a century ago (Van Engelen, 2019). Its core principle is to introduce a low-friction interface that decouples the structure from its foundation, thereby dissipating seismic energy and lengthening the structure's fundamental period. Over the past few decades, the development of base isolation technology has garnered significant attention and has become a widely adopted strategy for mitigating earthquake-induced damage in high-seismicity regions. Numerous researchers have contributed to the design of reliable devices that create a flexible isolation layer while maintaining high vertical stiffness. Technological advances have led to the emergence of innovative isolation systems, most of which fall into two main categories: elastomeric isolators and curved sliding surface isolators.

Elastomeric isolators exploit the deformability of elastomeric materials, which are well-suited for base isolation due to their low shear modulus and capacity for large, reversible strains. In contrast, sliding isolators rely on the relative motion between low-friction surfaces to absorb seismic energy and reduce transmitted forces (De Domenico, 2020; Furinghetti, 2021).

1.1. Historical Background

The earliest documented concepts of base isolation appeared in the late 19th and early 20th centuries, driven by the growing need to protect essential structures from the destructive effects of earthquakes. One of the first known patents for a base isolation system was filed in 1870 by British seismologist John Milne, who proposed the use of sand layers placed between the structure and its foundation to absorb seismic energy. Although rudimentary, this idea laid the foundation for the development of more advanced isolation techniques.

By the mid-20th century, the global engineering community began to seriously address the seismic vulnerability of buildings. Major earthquakes in Japan, Italy, and California highlighted the limitations of conventional structural systems. It became increasingly clear that traditional approaches were insufficient, particularly for tall and flexible buildings, which often sustained considerable damage despite meeting strength requirements.

1.2. Methodology

The concept of base isolation involves decoupling the entire structure—or selected components of it—from the ground by introducing flexible elements along a designated isolation interface. The objective is to concentrate all seismic-

induced deformations within these flexible elements, thereby enabling the superstructure to behave essentially as a rigid body.

This strategy increases the structure's fundamental period, shifting it away from the dominant frequency range of potential ground motions at the site. While a longer period results in larger displacements, these can be accommodated by ensuring adequate clearance around the isolation system. At the same time, extending the period leads to a significant reduction in the seismic base shear acting on the structure (Naeim and Kelly, 1999).

The selection and implementation of an appropriate isolation scheme depend on multiple factors, including the structural typology, the number and configuration of isolation devices (which directly influences cost), and the desired performance objectives (Cheng *et al.*, 2008). The core principle of base isolation is to alter the dynamic response of the structure so that ground motion can occur with minimal transmission to the superstructure. Ideally, the system would achieve complete decoupling; however, in practice, some contact points between the superstructure and the ground are necessary to maintain vertical load transfer and overall stability.

The incorporation of seismic isolators increases the horizontal flexibility at the base of the structure, with the primary goal of lengthening the vibration period and thereby significantly reducing the acceleration transmitted to the superstructure (Bratu, 2021). A comparison of displacement and force demands reveals that as the vibration period increases, base-level displacements rise while the forces acting on the structure decrease (D'Amato *et al.*, 2020).

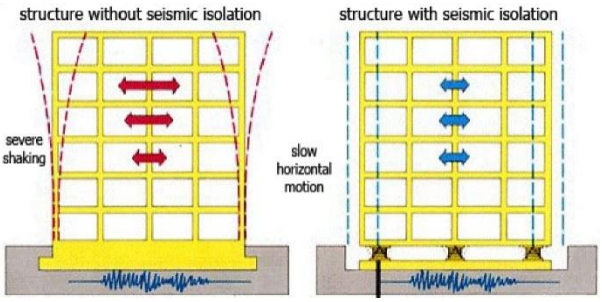

Fig. 1. Seismic Response of a Structure with and without Base Isolation (Polat, 2017).

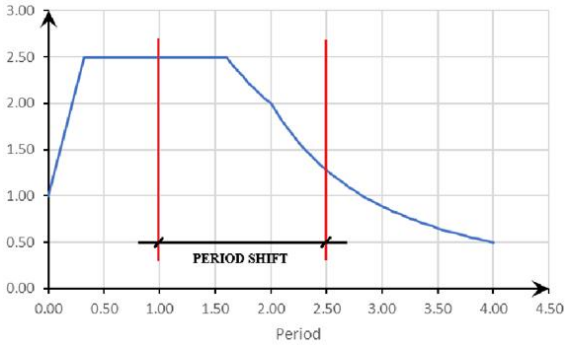

Fig. 2. The Theoretical Principle of Base Isolation – Period Shift.

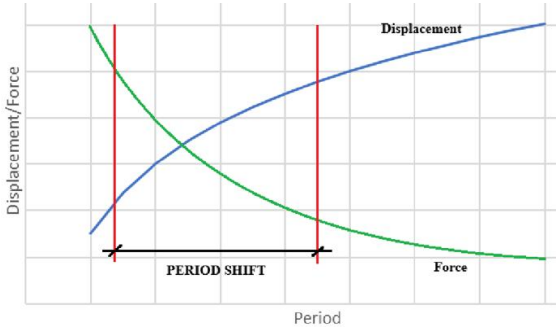

Fig. 3. The Theoretical Principle of Base Isolation- Period Shift vs. Force / Displacement.

Fig. 1, Fig. 2 and Fig. 3 illustrate the base isolation concept and highlight the key advantages of an isolated structural system: reduced inter-story drifts, limited deformations, and lightly loaded structural elements (Marioni, 2024). Owing to the low lateral stiffness introduced by the isolation layer, the fundamental period of the isolated structure becomes substantially longer than that of its fixed-base counterpart.

This period elongation results in a marked reduction in seismic accelerations—and, consequently, in the inertial forces transmitted to the structure (Bratu *et al*., 2024a; Bratu *et al*., 2024c).

1.3. Types of Isolators

Base isolation systems are widely recognized as efficient and practical solutions for protecting both structural and non-structural components from seismic hazards (Ramavath, 2024; Nawaz and Mohan, 2023; Nawaz and Mohan, 2024). However, during severe seismic events, excessive displacements may occur, potentially leading to damage in both the isolators and the structure itself. Recent advances in seismic isolation technology have prompted the development of innovative systems exhibiting adaptive behavior. A device is considered adaptive when its mechanical properties—such as stiffness or damping—vary significantly in response to the level of stress (Bratu *et al*., 2024b). This allows the device to adjust its response based on the intensity of the seismic input, typically starting with an initial soft (relaxation) phase followed by stiffening and/or increased damping as displacements grow.

In recent years, the concept of adaptivity has gained considerable attention within the research community. Certain adaptive devices demonstrate a high capacity for energy dissipation under strong ground motions, contributing to reduced floor accelerations and lower inter-story drifts across a broad range of seismic intensities. Others are particularly effective in mitigating responses under low-to-moderate seismic activity, while still maintaining displacement control during extreme events (Sheikh *et al*., 2022).

Traditional base isolation systems, by contrast, suffer from an inherent limitation: lack of adaptability. They are typically optimized for a specific range of ground motion characteristics and may underperform when subjected to seismic events outside those design parameters (Bao, 2018; Lu, 2013).

Conventional, non-adaptive base isolation systems typically rely on isolators that combine lateral flexibility with high vertical stiffness, ensuring effective control of horizontal seismic motions while maintaining gravity load-bearing capacity. Commonly used devices in such systems include (Marioni, 2024; Sabiha *et al*., 2023):

- Laminated rubber bearings with low damping (LDRB)
- Lead-core rubber bearings (LRB)
- High-damping rubber bearings (HDRB), made of synthetic rubber with inherent damping properties
- Sliding bearings (SB), which dissipate energy through friction between low-friction surfaces

2. Lead Rubber Bearings (LRB) - Elastomeric Isolation Devices

Lead-core rubber bearings (LRB), illustrated in Fig. 4, are structurally similar to low-damping rubber bearings (LDRB), but incorporate one or more lead cores to overcome some of the limitations associated with low intrinsic damping. To accommodate the lead core, a slightly undersized hole is typically drilled at the center of the bearing, ensuring tight contact between the core and the surrounding rubber layers. This configuration enables effective composite action between the elastomer and the lead insert. While LRBs are most commonly circular in shape, they can also be manufactured in rectangular formats to suit specific design requirements.

The integration of the lead core significantly enhances the isolator's energy dissipation capacity. During seismic excitation, the lead core undergoes plastic deformation, absorbing and dissipating additional energy. This mechanism improves the overall performance of the isolator by reducing the seismic forces transmitted to the structure and increasing its resilience to earthquake-induced damage.

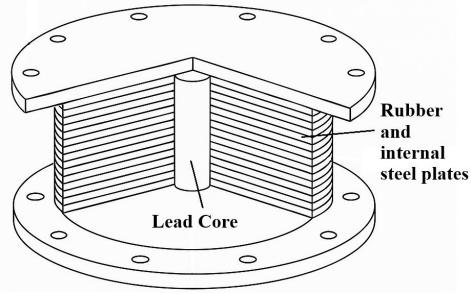

Fig. 4. LRB Isolator.

The performance of lead-core rubber bearings (LRB) is significantly influenced by the magnitude of lateral forces acting upon them. At low lateral force levels, the lead core constrains the motion of the internal steel plates, resulting in increased lateral stiffness. As the lateral force increases, the plates exert pressure on the lead core, causing it to deform plastically or shift, which introduces hysteretic damping through energy absorption in the lead. Consequently, the isolator's lateral stiffness decreases as its energy dissipation capacity increases.

The effective damping provided by LRBs typically ranges between 10% and 35%, depending on the applied force and displacement demands (Yao *et al*., 2024). To represent their nonlinear mechanical behavior under seismic loading, a bilinear model is commonly employed (Fig. 5). This simplified representation captures the key features of LRB performance and facilitates reliable predictions of structural response under earthquake excitation (Bhandari and Bharti, 2018; Afshar *et al*., 2023).

The bilinear behavior of lead-core isolators can generally be characterized by several key parameters, such as:

- k_e - initial stiffness, which represents the elastic stiffness,
- k_p - post-yield stiffness, indicating the stiffness of the isolator once it has yielded,
- Q - characteristic strength, used to evaluate the stability of hysteretic behavior during repeated loading cycles,
- k_{eff} - effective stiffness representing a mean stiffness value accounting for both k_e and k_p, typically used in dynamic analyses.

When a lateral force is applied to the isolator, its force–displacement response initially follows a linear relationship up to point "a", which is valid during both loading and unloading phases. In this elastic range, the stiffness is defined by the initial stiffness k_e. Upon reaching point "b", the yield strength F_y of the lead core is attained, beyond which the isolator experiences larger displacements with only marginal increases in force. In this post-yield region, the stiffness reduces to the post-yield stiffness k_p.

As the load begins to reverse (unloading phase), the response reverts to the initial stiffness k_e over an interval corresponding to 2 F_y. Beyond point "d", unloading continues with the reduced stiffness k_p, following the same bilinear pattern observed during loading.

This idealized bilinear model provides valuable insight into the dynamic behavior of lead-core isolators, particularly in high-seismic regions. It effectively captures both energy dissipation and flexible displacement control, enabling accurate assessment of

structural response across varying seismic force levels.

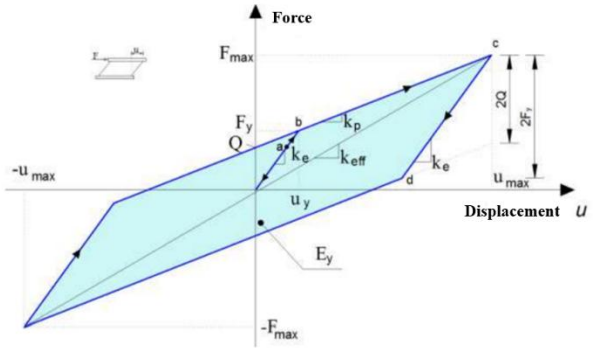

Fig. 5. Bilinear Force-Displacement Model of LRB.

The post-yield stiffness k_p is equal to:

$$k_p = \frac{A_b \cdot G \cdot f_l}{t_r} \quad (1)$$

where:

- A_b is the cross-sectional area of the isolator,
- G is the shear modulus of the rubber, typically ranging from 0.4 MPa to 1.0 MPa,
- $t_r = \sum t$, represents the cumulative thickness of all rubber layers,
- f_l is a correction factor for the presence of the metal plates. These limit the lateral deformation of the isolator and increase the shear resistance capacity.

The elastic stiffness of the isolator, k_e, can be approximated using a relationship between the post-elastic stiffness k_p and a predetermined interval, according to the formula:

$$6.5k_p \leq k_e \leq 10k_p \quad (2)$$

The characteristic strength Q of a lead core isolator can be calculated using the formula:

$$Q = A_p \sigma_y \quad (3)$$

in which:

- A_p represents the cross-sectional area of the lead core, which is dependent on the physical dimensions of the cylindrical core,
- σ_y denotes the yield stress of the lead, which varies based on the type of lead which is utilized, the vertical load applied, and the confinement of the lead core. Typical values for the lead used in isolators range from 10 to 15 MPa.

The yield displacement, u_y, is calculated as a function of k_p and k_e as follows:

$$u_y = \frac{Q}{k_e - k_p} \quad (4)$$

The yield force F_y at the yield displacement u_y, is:

$$F_y = Q + k_p u_y \quad (5)$$

The effective damping of the isolator is calculated using the relationship:

$$\xi_{eff} = \frac{2Q(u_{max} - u_y)}{\pi k_{eff} D_{max}^2} \quad (6)$$

where:

- u_{max} is the maximum displacement of the isolator under load,
- D_{max} is the maximum displacement attained by the isolated structure,
- k_{eff} is the effective stiffness of the isolator.

The formula for calculating the effective stiffness, k_{eff} is:

$$k_{eff} = \frac{Q + k_p u_y}{u_{max}} \quad (7)$$

In dynamic analyses of seismically isolated structures, the effective stiffness k_{eff} of the isolation system is typically used to compute the global structural response. This approach enables a more realistic modeling of the isolator's behavior, accounting for both the elastic and post-elastic phases, as well as for the energy dissipation occurring within the system.

Elastomeric base isolation systems offer numerous advantages, with the most significant being the substantial reduction of structural and non-structural damage during seismic events. This performance is achieved through the reduction of seismic forces transmitted from the ground to the superstructure, and through hysteretic damping mechanisms that dissipate seismic energy efficiently, thereby limiting structural vibrations. As a result, base-isolated structures often remain functional following earthquakes—a critical requirement for essential facilities such as hospitals, emergency response centers, and infrastructure networks.

Elastomeric devices can be employed in both new constructions and retrofitted into existing buildings. Materials used for hysteretic damping, such as lead or steel, are known for their long service life and capacity to endure repeated deformation cycles without significant degradation.

Despite their benefits, base isolation systems are not without limitations. These include higher initial costs compared to conventional construction techniques, as well as additional spatial requirements around the isolated building to accommodate the increased lateral displacements during seismic events. Furthermore, while elastomeric isolators are effective in attenuating horizontal ground motions, they offer limited protection against strong vertical accelerations.

3. Establishing the Input Data for The Model

The structure analyzed in this study is representative of a typical office building located in the Municipality of Bucharest. The building features a height configuration of ground floor plus five stories (GF + 5F), with a ground floor height of 4 meters and a height of 3 meters for each of the upper floors. In plan, the building measures 18 meters by 15 meters, comprising three spans of 6 meters and three bays of 5 meters. The layout is regular and symmetrically aligned along both principal axes, as illustrated in Fig. 6.

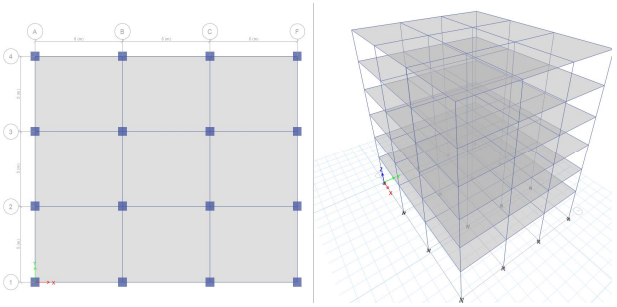

Fig. 6. Configuration of the Analyzed Structure.

To highlight the differences in structural behavior between the fixed-base and base-isolated configurations, numerical analyses were performed using ETABS, version 18.0.2.

3.1. Data Regarding the Site

The construction site, in accordance with the Romanian seismic design code P100-1/ 2013, is characterized by a design ground acceleration a_g=0.30g, corresponding to earthquakes with a mean recurrence interval of 225 years and a 20% probability of exceedance over a 50-year period. The value of the corner period is T_c=1.6s, with the normalized elastic response spectrum β(T) equal to β_0=2.50.

The construction is included in the importance-exposure class III.

In terms of the snow load, according to the Romanian standard CR 1-1-3/ 2012, the site corresponds to a characteristic ground snow load value of $s_{0,k}$=2kN / m^2, with a mean recurrence interval of 50 years.

3.2. Technical Description of the Structure

The structural solution was achieved by adopting a frame-type system, with the following dimensions for:

- Beams: 30 x 60 cm,
- Columns: 60 x 60 cm,
- Slabs: thickness of 13 cm.

The structural frame was constructed using concrete of class C30/37.

3.3. Technical Description of the Structure

The seismic action was modeled using the response spectrum method. The analysis accounted for the simultaneous effects of the two horizontal components of seismic motion by employing the following load combinations: $E_{Edx}+0.30E_{Edy}$ and $0.30E_{Edx} + E_{Edy}$, where:

- E_{Edx} represents the application of the seismic motion in the horizontal x-direction considered for the structure,
- E_{Edy} represents the application of the seismic motion in the horizontal y-direction considered for the structure.

The loads assessed for the structural model are shown below, in Table 1.

Table 1. Types and Characteristic Values for the Considered Loads.

No.	Load Type	Value [unit]
1.	Snow	1.60 *kN/m²*
2.	Live Load for Non-Traffic Terrace	0.40 *kN/m²*
3.	Live Load for Current Floor	2.00 *kN/m²*
4.	Finishes	0.50 *kN/m²*
5.	Partition Walls	0.50 *kN/m²*
6.	Exterior Walls	5.25 *kN/m*
7.	Attic	2.75 *kN/m*

3.4. Calculation of the Isolator Parameters

To analyze the improvements brought by a base isolation system on the structural response, the necessary parameters were calculated for the introduction of the selected LRB type isolator into the ETABS program, following an assessment of several variants with different values of stiffness and maximum displacements.

Thus, for the chosen isolator, the following data were obtained and shown in Table 2.

Table 2. Characteristics of the Considered Isolator.

Parameter	Symbol	Value	Unit
Cross-Sectional Area of Isolator	A_b	0.6	*m²*
Shear Modulus of the Rubber	G	0.8	*MPa*
Total Thickness of the Rubber Layers	t_r	0.15	*m*
Correction Factor for the Metal Plates	f_l	1.2	-
Post-Elastic Stiffness	k_p	97.65	*kN/m*
Elastic Stiffness	k_e	30000	*kN/m*
Cross-Sectional Area of the Lead Core	A_p	0.02	*m²*
Yield Stress of the Lead	σ_y	12	*MPa*
Characteristic Strength	Q	240	*kN*
Displacement at the Yield Limit	u_y	2.45	*m*
Yield Force	F_y	480	*kN*
Maximum Isolator Displacement	u_{max}	0.15	*m*
Effective Stiffness	k_{eff}	1697.65	*kN/m*
Maximum Structural Displacement	D_{max}	0.3	*m*
Effective Damping	ξ_{eff}	0.15	15%

3.5. Considered Scenarios

Given the current context, characterized by extensive armed conflicts and terrorist threats primarily targeting the destruction of specific buildings, alongside the seismic action, this study proposes a structural analysis for an extreme explosive load.

It is assumed that an explosive charge of 50 kg TNT is initiated at a distance of 10 m from one of the building's facades and 1 m above the ground level, Fig. 7. The detonation will generate a shock wave

that dynamically loads the structural elements of the exposed facade.

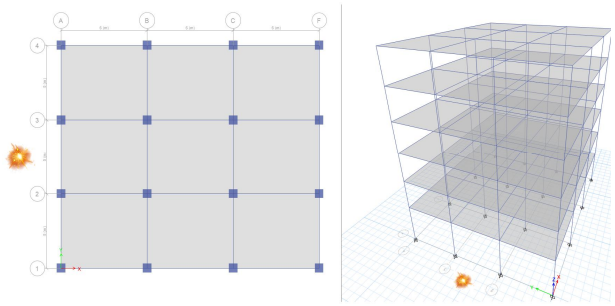

Fig. 7. Load Arrangement.

The analysis considered two loading scenarios for both the structure with and without base isolation:

a) Scenario 1A: seismic action corresponding to an earthquake with maximum intensity at the considered site – structure fixed to the ground (without base isolation);

b) Scenario 1B: the same seismic action – structure with base isolation;

c) Scenario 2A: external explosion – structure fixed to the ground (without base isolation);

d) Scenario 2B: external explosion – structure with base isolation.

3.6. Blast Type Action

The manifestation of the shock wave generated by the initiation of the explosive charge on a building is a complex phenomenon that requires explanation.

The shock wave is primarily characterized by the evolution of the overpressure over time, as illustrated in Fig. 8. Since the shock waves are not sustained, they dissipate as they move away from the explosion point until the pressure generated by the explosion equalizes with atmospheric pressure. Alongside the overpressure value, the distinctiveness of each shock wave is defined by two additional characteristics: the duration of the shock wave's action, tp, and the impulse (force-time product) per unit area for the forces exerted by the blast. It is also essential to know the arrival time, ts (the time required for the shock wave to travel from the detonation point to the target) (Lupoae and Baciu, 2016).

To determine the overpressure at the front of the shock wave for an explosion in air, several experimentally established calculation relationships can be used.

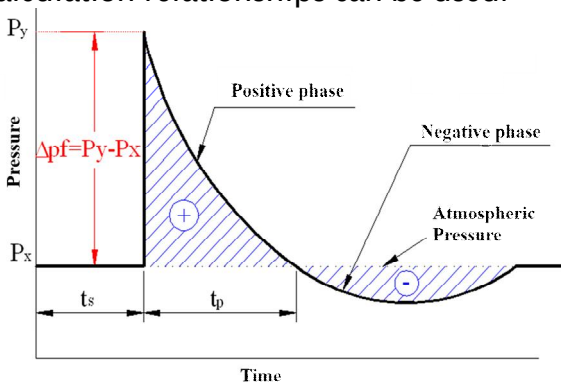

Fig. 8. Pressure-Time Curve for a Shock Wave in Air (Lupoae and Baciu, 2016).

The equation presented by Kinney is the most frequently employed, as referenced in [9], Δ_{pf} having the expression listed below, with results expressed in bars:

$$\Delta p_f = \frac{808\cdot\left[1+\left(\frac{Z}{4.5}\right)^2\right]\cdot P_a}{\sqrt{1+\left(\frac{Z}{0.048}\right)^2}\cdot\sqrt{1+\left(\frac{Z}{0.32}\right)^2}\cdot\sqrt{1+\left(\frac{Z}{1.35}\right)^2}}, \quad (8)$$

where:

- Δ_{pf} is the overpressure (in Pascals),
- P_a is the atmospheric pressure,
- Z is the scaled distance, defined as $Z=R/W^{1/3}$, in which R represents the distance in meters between the explosive charge and the target and W is the mass of the explosive charge in kilograms.

In the event that an explosion occurs in close proximity to the ground, the reflection phenomenon leads to an increase in the pressure measured at the level of an exposed surface. The reflected

pressure can be calculated using the formula:

$$p_r = 2\Delta p_f \frac{7 \cdot P_a + 4 \cdot \Delta p_f}{7 \cdot P_a + \Delta p_f} \quad (9)$$

The loading mode of a building exposed to an explosion is detailed in the following figure, Fig. 9.

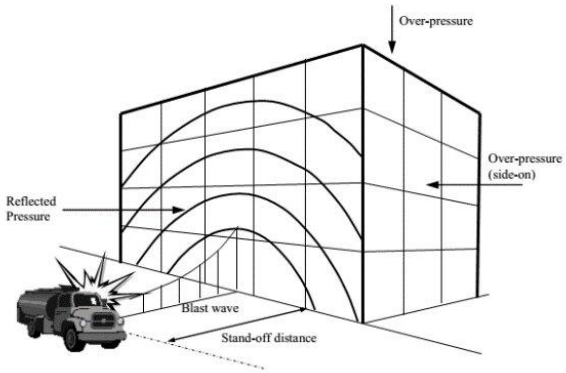

Fig. 9. Explosion Loading on a Building (Abbas and Adil, 2018).

For the analyzed structure, the pressure values assigned to each structural element of the exposed façade were determined based on the distance from the explosion site, Fig. 10.

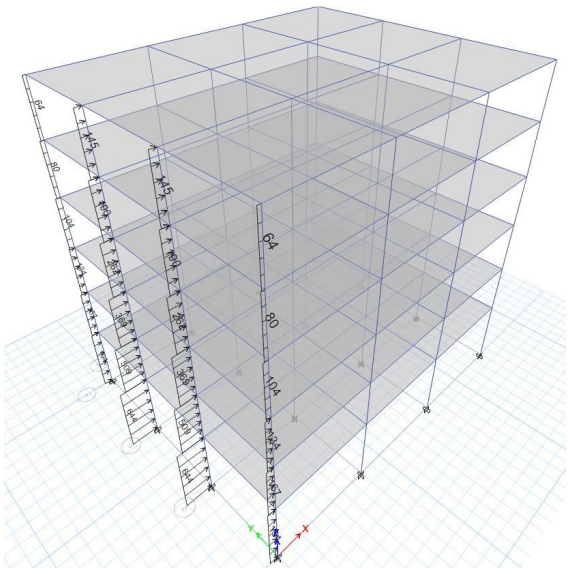

Fig. 10. Modeling the Effects of Explosion on the Structural Elements of the Exposed Façade.

Since the duration of the reflected pressure on the exposed façade of the building is very short (on the order of milliseconds), the proposed analysis method is dynamic-linear. Thus, a time-history function, Fig. 11, was generated to capture the dynamic response of the structure. The calculations yielded a value for the duration of the positive phase, t_p = 9.7ms.

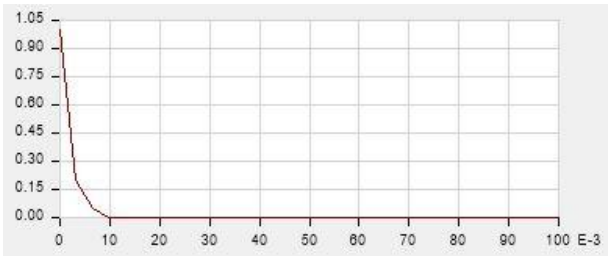

Fig. 11. Time Function Introduced to Capture the Positive Phase of the Explosion.

Additionally, the calculated speed of the shock wave at the level of the exposed façade is approximately 640 m/s, which is nearly double the speed of sound (343m/s).

4. Results

In the case of scenario 1A, when the structure is considered fixed at the ground level, the vibration modes and corresponding mass participation factors have been established in accordance with the provisions of the seismic design code P100-1/ 2013. This assessment takes into account the rigidity of the reinforced concrete elements, which has been reduced by half. The results are shown in Table 3.

Table 3. Vibration Modes, Scenario 1A.

Mode	Type	Period [s]	Participating mass [%]
1	Translation–Ox direction	0.89	85.70
2	Translation–Oy direction	0.85	86.20
3	Torsion	0.76	86.20

It is observed that the choice of a regular structure in both plan and elevation,

symmetric along both principal directions, results in an organized modal response, with the mass predominantly participating in the fundamental mode. This aspect was considered to better capture the effects generated by the introduction of the isolators.

In the case of scenario 1B, where the structure has an isolated base, the vibration modes and mass participation factors have been established for the full rigidity of the elements (we anticipate that the structural elements will not crack, as they are subjected to significantly lower stresses compared to the fixed-base structure). The results are shown in Table 4.

Table 4. Vibration Modes, Scenario 1B.

Mode	Type	Period [s]	Participating mass [%]
1	Translation–Ox direction	2.10	99.80
2	Translation–Oy direction	2.08	99.80
3	Torsion	1.87	99.80

As expected, the fundamental period of the structure increases significantly following the decoupling from the ground. Additionally, the motion of the structure during dynamic loading becomes much more organized: while approximately 15% of the participating mass in the fixed-base structure corresponds to higher vibration modes, in the structure with isolators, the contribution of the first vibration mode to the structural response is practically total.

4.1. Displacements and Story Drifts

The selected structure for the analysis was evaluated considering the relative story drifts with respect to the height of the level, both at the Serviceability Limit State (SLS), Fig. 12, and the Ultimate Limit State (ULS), Fig. 13, in accordance with the provisions outlined in the Seismic Code.

As expected, a six-story structure located in Bucharest, configured solely as a reinforced concrete frame without structural walls, will not meet the requirements imposed by the current regulations regarding displacements.

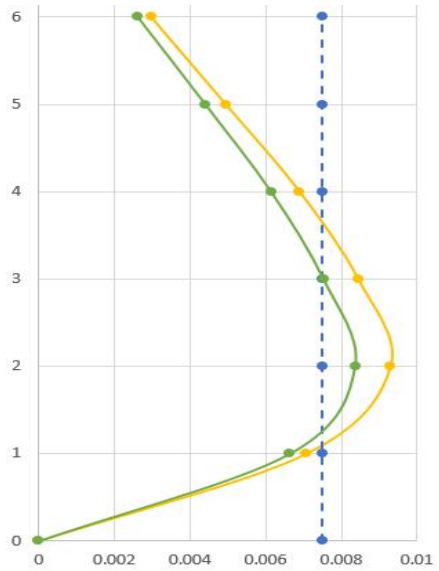

Fig. 12. Distribution of the Drift along the Height of the Structure in Both Directions, Scenario 1A – SLS.

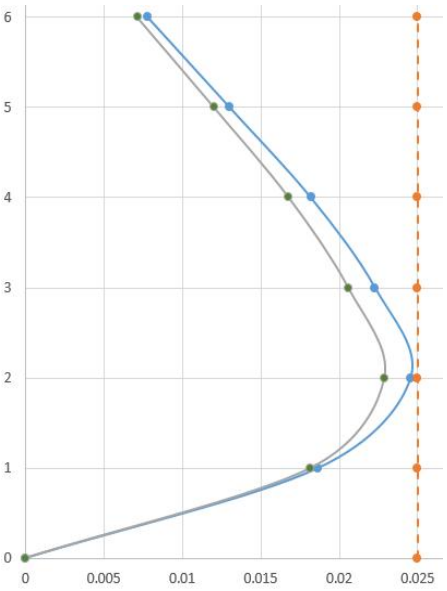

Fig. 13. Distribution of the Drift along the Height of the Structure in Both Directions, Scenario 1A – SLU.

It is observed that for Scenario 1A, at the Ultimate Limit State, the drift values are

very close to the maximum allowable limits, Fig. 13. However, in the case of the Serviceability Limit State, the drift values significantly exceed the corresponding limits Fig. 12.

For the structure with seismic isolators in Scenario 1B, the relative displacements between levels decrease significantly, with the structure essentially translating as a whole in the lateral directions. Fig. 14 shows that the drift values are much lower this time compared to the 0.75% limit imposed by the Serviceability Limit State. The drifts in Scenario 1B are at least 10 times smaller than those obtained for Scenario 1A. Additionally, it is noted that the maximum drift values for a fixed-base structure (Scenario 1A) occur at a level situated approximately one-third of the height from the base, whereas for a structure with an isolated base, the maximum drifts occur at the base and decrease with the height.

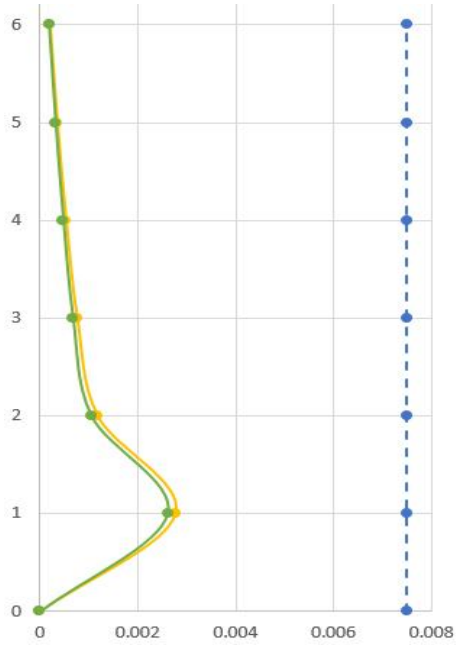

Fig. 14. Distribution of the Drift along the Height of the Structure in Both Directions, Scenario 1B.

From the perspective of the maximum displacements obtained for a reference point at the top level, the results are presented in Table 5. Only the maximum displacement in the x-direction (Ox) was considered, allowing for the inclusion of displacements resulting from the explosion scenarios as well.

Table 5. Maximum Displacements at the Upper Level.

Scenario	Maximum Displacement [mm]
1A	330
1B	92
2A	2.40
2B	8

The maximum displacement value for scenario 1A was determined considering the conditions corresponding to the ultimate limit state (accounting for the degradation of the elements' stiffness). For the fixed-base structure, the inter-level displacements increase from a value of 0 at the base to a maximum value of approximately 330 mm at the top level. In the case of the base-isolated structure (scenario 1B), the displacement at the base is no longer zero, with a measured displacement of 73 mm; as one moves up the height of the structure, these displacements increase, but at a much lower rate compared to scenario 1A, reaching a maximum value of 92 mm. The difference between the displacement at the top level and the base is only 19 mm, confirming that the structural elements are subjected to much lower demands, effectively retaining their near-full stiffness.

For the explosion loading cases, the structural responses are given over time. To limit the computation time, the dynamic analysis was set for a duration of 3 seconds (after which only the free vibrations of the structure occur).

For the case of the fixed-base structure (scenario 2A), the maximum

displacement is 1.2 mm at the first level and 2.40 mm at the top level (value obtained at the time step of 0.45s), as shown in Fig. 15. In the case of the base-isolated structure (scenario 2B), a response characterized by significantly longer periods is observed, attributed to the action mechanism of the isolators, Fig. 16. In this case, the maximum displacement at the first level is 7.22 mm, while at the top level it reaches 8.17 mm, occurring at the time step of 1.54s.

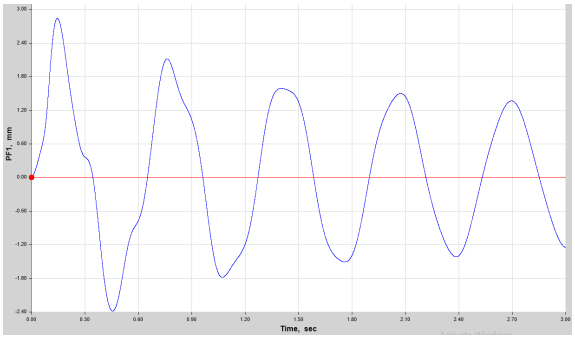

Fig. 15. Time Variation of the Displacement in the Ox Direction of a Point at the Upper Level - Scenario 2A.

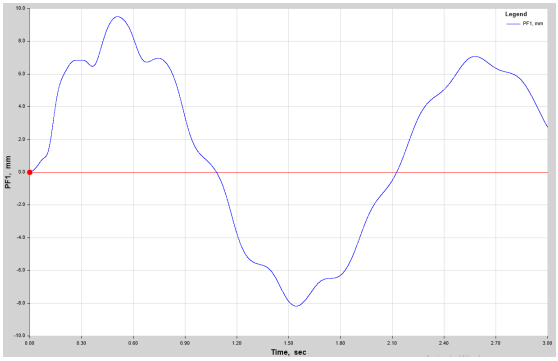

Fig. 16. Time Variation of the Displacement in the Ox Direction of a Point at the Upper Level - Scenario 2B.

4.2. Base Shear Force

The structural analysis also includes a comparison of the base shear values: higher values are obtained for the fixed-base structure (comparing scenarios 1A and 1B, as well as 2A and 2B). Although the forces distributed on the columns of the facade exposed to the explosion (scenarios 2A and 2B) would sum to a total lateral push exceeding 5700kN in the static case, the results obtained yield significantly lower values. This reduction is primarily due to the fact that these forces are applied dynamically over a very short duration of only 9.7 milliseconds. The values of the base shear forces are show in Table 6.

Table 6. Base Shear Forces.

Scenario	Base Shear Force [kN]
1A	1584
1B	1288
2A	432
2B	128

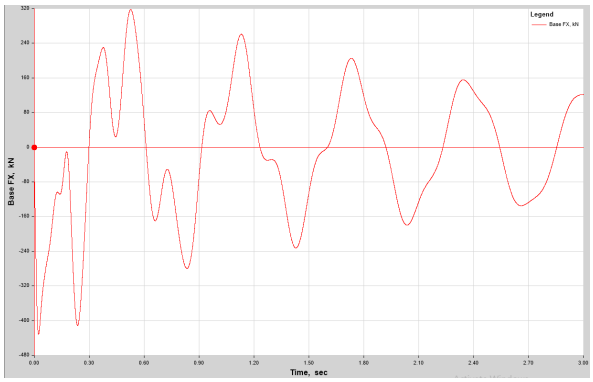

Fig. 17. Time Variation over time of the base shear force in the Ox direction - Scenario 2A.

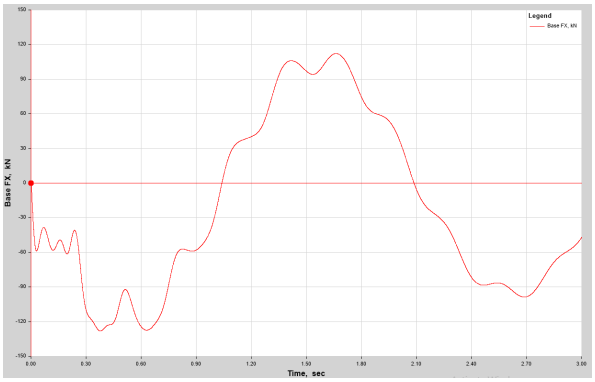

Fig. 18. Time Variation over time of the base shear force in the Ox direction - Scenario 2B.

The graphs depicting the variation of the base shear force for the explosion loading cases once again highlight that the isolators lead to a distribution characterized by longer periods, similar to the observed deformations.

The maximum base shear force for scenario 2A, Fig. 17, is 432kN, achieved at a time step of 0.023 seconds (thus, almost at the moment of the explosion initiation), whereas for scenario 2B, Fig. 18, the maximum value of 128kN is reached at a time step of 0.37 seconds. Essentially, the impact of the initial shock is significantly reduced when utilizing isolators.

5. Conclusions

The present study aimed to evaluate the influence of seismic base isolators on a regular reinforced concrete frame structure subjected to extreme actions—namely seismic events and explosions. Although the energy dissipation characteristics of isolators are specifically designed for the frequency content of seismic ground motions, the analyses demonstrated that these devices also mitigate the effects of explosions in terms of displacements, internal forces, and their time-dependent variation.

Buildings considered vulnerable to terrorist actions can be designed with base isolation in combination with additional dissipation systems installed between the façades and the structural frame.

The comparative analysis of the four proposed scenarios led to several important observations. Inter-story drifts and maximum displacements decreased significantly when isolators were used. The development of lateral displacements along the building height was characterized by a predominantly translational motion in the isolated-base configuration, with much smaller joint rotations. Furthermore, the evaluation of vibration modes and modal mass participation ratios revealed a substantial increase in the fundamental vibration period for the isolated structure, as well as a more ordered oscillatory motion, with the fundamental mode contributing almost entirely to the structural response.

The results also confirmed that, for a six-story reinforced concrete frame structure located in Bucharest, a conventional fixed-base configuration is not an adequate seismic solution. Meeting the displacement limits prescribed by design codes would require the addition of structural walls in both principal directions to increase the global stiffness. However, when the same frame structure is decoupled from the ground through base isolation, the inclusion of walls is no longer mandatory.

Dynamic analyses based on time-history functions for blast scenarios provided insight into the temporal evolution of deformations, base shear forces, and internal stresses. The presence of isolators resulted in longer-period structural responses, reducing the occurrence of sudden force variations typically responsible for local damage in structural elements.

Although the analyses performed provide valuable insight into the structural response of base-isolated buildings subjected to both seismic and blast actions, certain limitations must be acknowledged, particularly regarding the applicability of isolation systems to explosion scenarios. The response of elastomeric bearings is governed by their inherent viscoelastic properties, which require a minimum activation time to develop significant deformation and damping capacity. In the case of blast loads—characterized by extremely short positive pressure phases, on the order of milliseconds—this response interval may be insufficient for the isolators to fully engage their energy dissipation mechanisms. Consequently, the beneficial effects observed in this study should be

interpreted as indicative trends rather than definitive performance predictions.

Further research involving nonlinear time-history analyses, advanced constitutive models for elastomeric materials and experimental validation under impulsive loading are needed to more accurately quantify the real efficiency of base isolation systems in blast scenarios.

REFERENCES

Abbas A., Adil M. (2018), *Behavior of reinforced concrete sandwiched panels (RCSPs) under blast load*, Engineering Structures 181(1): 476-490, DOI:10.1016/j.engstruct.2018.12.051.

Afshar M. A., Aghaeipour S., Adlparvar M., Mazloum A. A. (2023), *Optimal dynamic performance of partially Base-Isolated structure under seismic Excitations: Harmonic, Earthquake, and random*, Structures 55(1): 263-277, DOI:10.1016/j.istruc.2023.05.110.

Bao Y. (2018), *Inelastic response of base-isolated structures subjected to impact*, Engineering Structures 171(1): 86-93, DOI:10.1016/j.engstruct.2018.05.091.

Bhandari M., Bharti S. D. (2018), *Assessment of proposed lateral load patterns in pushover analysis for base-isolated frames*, Engineering Structures 175(1): 531-548, DOI:10.1016/j.engstruct.2018.08.080.

Bratu P. (2021), *Dynamic isolation. Vibrational and seismic actions* [*Izolarea dinamica. Actiuni vibratorii si seismice*], Editura Impuls, Bucharest, Romania.

Bratu P., Dragomir C. S., Dobre D. (2024), *Assessment of the compound damping of a system with parallelly coupled anti-seismic devices*, Buildings 14(8): 2422, DOI:10.3390/buildings14082422.

Bratu P., Murzea P., Tonciu O., Dragan N., Dobrescu C. F. (2024), *Evaluation of the dynamic parameters under seismic conditions for a Maxwell rheological base isolation system*, Buildings 14(12): 4075, DOI:10.3390/buildings14124075.

Bratu P., Tonciu O., Dobrescu C. F., Vasile O. (2024), *The dynamic response of the vibrating system in the case of the Maxwell rheological model*, Acoustics and Vibration of Mechanical Structures 302(1): 253-259, DOI: 10.1007/978-3-031-48087-4_27.

Cheng F. Y., Jiang H., Lou K. (2008), *Smart structures innovative systems for seismic response control*, CRC Press Taylor & Francis Group, Boca Raton, Florida, SUA.

D'Amato M., Laguardia R., Gigliotti R. (2020), *Seismic retrofit of an existing RC building with isolation devices applied at base*, Frontiers in Built Environment 6(1): 82, DOI:10.3389/fbuil.2020.00082.

De Domenico D. (2020), *Adaptive isolation system combining low-friction sliding pendulum bearings and SMA-based gap dampers,* Engineering Structures 212(1): 110536, DOI:10.1016/j.engstruct.2020.110536.

Furinghetti M. (2021), *Experimental evaluation of extra-stroke displacement capacity for curved surface slider devices*, Soil Dynamics and Earthquake Engineering 146(1): 106752, DOI:10.1016/j.soildyn.2021.106752.

Kinney G. F., Graham K. I. (1985), *Explosive shocks in air*, Springer-Verlag, Berlin, Germany.

Lu L.-Y. (2013), *Experimental evaluation of supplemental viscous damping for a sliding isolation system under pulse-like base excitations*, Journal of Sound and Vibration 332(8): 1982-1999, DOI:10.1016/j.jsv.2012.12.008.

Lupoae M., Baciu C. (2016), *Effects of extreme loads on constructions* [*Efectele încărcărilor extreme asupra construcțiilor*], Editura Academiei Tehnice Militare, Bucharest, Romania.

Marioni A. (2024), *Anti-Seismic Devices: A Reference Manual for Structural Engineers*, Springer, Cham, Switzerland.

Naeim F., Kelly J. M. (1999), *Design of seismic isolated structures – from theory to practice*, John Wiley & Sons Inc., New York, SUA.

Nawaz Z., Mohan S. (2023), *Development of low-cost base isolation technique using multi-criteria optimization and its application to masonry building*, Soil Dynamics and Earthquake Engineering 172(1): 108024, DOI: 10.1016/j.soildyn.2023.108024.

Nawaz Z., Mohan S. (2024), *Performance of low-cost unreinforced elastomeric isolator for masonry building: Experimental investigations and numerical analysis,* Structures 63(4): 106365, DOI:10.1016/j.istruc.2024.106365.

Polat H. I. (2017), *Analysis of a frame-shear wall concrete structure by using base isolation and evaluation of structure-soil interaction*, Engineering, Technology & Applied Science Research 7(6): 2282-2287, DOI:10.48084/etasr.1611.

Ramavath R. (2024), *Base Isolation and Energy Dissipating System in Earthquake Resistant Building Design*, CVR Journal of Science

and Technology 26(1): 13-20, DOI: 10.32377/cvrjst2603.

Ranbeer T., Aditya K. -T. (2023), *Comparative study on the effectiveness of fluid viscous dampers and base isolation: An approach toward enhancing seismic performance of composite structures*, Innovative Infrastructure Solutions 8(10): 267, DOI:10.1007/s41062-023-01229-z.

Sabiha H., Lyacine B., Kernou N. (2023), *Comparative Study of the Non-Linear Dynamic Behaviour of Different Seismic Isolation Systems,* Advanced Engineering Forum 48(1): 17-29, DOI:10.4028/p-97i58z.

Sheikh H., Van Engelen N. C., Ruparathna R. (2022), *A review of base isolation systems with adaptive characteristics,* Structures 38(1): 1542-1555, DOI:10.1016/j.istruc.2022.02.067.

Van Engelen N. C. (2019), *Fiber-reinforced elastomeric isolators: a review*, Soil Dynamics and Earthquake Engineering 125(1): 105621, DOI:10.1016/j.soildyn.2019.03.035.

Yao D., Mohit B., Murtaza H. (2024), *Seismic response of base-isolated buildings: Exploring isolator properties*, Asian Journal of Civil Engineering 25(5): 4197-4209, DOI:10.1007/s42107-024-01041-9.

Received: 25 July 2025 • Revised: 5 November 2025 • Accepted: 10 November 2025